Optik - International Journal for Light and Electron Optics 200 (2020) 163419

Contents lists available at ScienceDirect

Optik

journal homepage: www.elsevier.com/locate/ijleo

Original research article

Simulations and experiments on the noise suppression in the calibration of a 961-element adaptive optics system

Cheng Xue[a,b,c,d], Wang Jianli[b], Wang Liang[b,*], Liu Xinyue[b], Dong Lei[b,c], Liu Changhua[b,c]

[a] Suzhou Institute of Biomedical Engineering and Technology, Chinese Academy of Sciences, Suzhou 215163, China
[b] Changchun Institute of Optics, Fine Mechanics and Physics, Chinese Academy of Sciences, Changchun, Jilin 130033, China
[c] University of Chinese Academy of Sciences, Beijing 100049, China
[d] Changchun Guoke Medical Engineering and Technology Development Co., Ltd, Changchun 130000, China

ARTICLE INFO

Keywords:
High-order adaptive optics system
Deformable mirror
Shack-Hartmann wavefront sensor
Influence matrix
Spatial-domain filter

ABSTRACT

Traditionally, the calibration matrix of a high-order adaptive optics system often suffers from the high noise, when the traditional push-pull calibration strategy is used. In this paper, taking a 961-element adaptive optics system as an example, the influence of calibration noise on the calibration matrix is analyzed, and the effects of filtering the influence matrix in the spatial domain are evaluated by numerical simulation, respectively. Finally, an experiment is conducted in the 961-element adaptive optics system and the results prove that filtering in the spatial domain is effective for the suppression of calibration noise.

1. Introduction

High-order adaptive optics (HOAO) is usually an indispensable part of large ground-based astronomical telescopes, for HOAO is useful in compensating the effects of atmospheric turbulence. For example, HOAO ensures high quality of high-contrast imaging [1], and therefore, enables direct imaging of extra-solar planets [2], which is one of the most challenging themes in today's astronomy.

Generally, in a HOAO system, a high-order deformable mirror (DM) and Shack-Hartmann wavefront sensor (SHWFS) are required, which correspond to a substantial number of actuators and subapertures, respectively. The calibration process, which should be carried out before HOAO correction, determines the relationship between the DM and SHWFS; to be more specific, this process measures the influence of the SHWFS when each actuator of the DM is actuated, and finally the influence matrix (IM) is measured. Traditionally, the IM is measured by using a push-and-pull method, that is to say, pushing and pulling the actuators one by one [3]. In this method, each push and pull measures the influence vector of a certain actuator, and all the influence vectors compose the influence matrix. However, in a HOAO system, with the number of subapertures increasing considerably, the majority elements of an influence vector are merely noise when the traditional push-and-pull method is adopted, which may probably lower the performance of a HOAO system. A review made by J. Kolb on the calibration of adaptive optics can be referred [4].

With the development and the application of the deformable secondary mirror in large ground-based telescopes, more calibration strategies are proposed and validated to improve the traditional push-and-pull calibration method [5–8]. M. Kasper proposed an optimized calibration method based on Hadamard pattern, which can reduce calibration time considerably [5]. On the basis of the method of M. Kasper, Y. Guo combined multichannel calibration method with the Hadamard actuation scheme and proposed a

* Corresponding author.
E-mail address: wangliang.ciomp@foxmail.com (L. Wang).

https://doi.org/10.1016/j.ijleo.2019.163419
Received 11 June 2019; Accepted 13 September 2019

multichannel Hadamard calibration method [6]. Also, Y. Guo proposed to obtain the influence matrix by direct computation [7]. S. Meimon believed that the maximum voltages, which is adopted in Hadamard actuation scheme, would be never adopted as channel voltage of DM for a closed-loop adaptive optics system in practice, and therefore, proposed a slope-oriented Hadamard calibration method [8]. Furthermore, based on a system identification approach, A. Chiuso proposed a dynamic calibration method [9]. In addition, C. T. Heritier introduced a pseudo synthetic approach, when a Pyramid WFS is adopted in HOAO system [10]. All these efforts have made great progress with HOAO calibration, however, little research focused on the effects of calibration noise. In this research, therefore, we focus on the effects of the noise in calibration and the methods of suppressing the noise. At first, taking the 961-element deformable mirror [11] as a example, we analyze the impact of the calibration noise on the influence matrix by using numerical simulation, and then, try to adopt a spatial-domain filtering method to suppress the calibration noise accordingly. Finally, we build up an experimental high-order adaptive optics system to validate this filtering method.

The rest of this paper is organized as follows. Section 2 describes the simulation of generating a influence matrix with noise and conducting a closed-loop wavefront correction with the influence matrix. Section 3 describes an experiment of closed-loop wavefront correction. Section 4 concludes this research.

2. Simulation of calibration and closed-loop wavefront correction

2.1. Adaptive optics system

In this section, we will construct a model of an adaptive optics system in order to conduct the numerical simulation of the calibration and closed-loop wavefront correction. The model is a compact adaptive optics system which is on the basis of the experimental system in Section 3. The model is composed of a Shack-Hartmann wavefront sensor, a deformable mirror, a calibration source. The DM is modeled according to the 961 piezo-actuator continuous-surface deformable mirror [11]. The diameter of the DM is 243 mm, the distance between neighboring actuator is 7 mm, and the coupling coefficient is about 23%. Here, coupling coefficient refers to the ratio of the deformation of the poked actuator to that of the neighboring actuator. The SHWFS adopts a lenslet array with a 7 mm focal length and a 200 μm lenslet pitch. The image sensor of the SHWFS is an industrial CCD camera, i.e. Basler® piA1000-60gm, with a 7.4 μm pixel size and a resolution of 1004 pixel × 1004 pixel. The camera works in the 2 pixel × 2 pixel binning mode. As is similar to our previous research of a 97-element adaptive optics system, the actuators of the DM and the subapertures of the SHWFS follows the Southwell configuration [12–14]. Under the framework of the Southwell configuration, one subaperture corresponds to one actuator, therefore, it will be more convenient to filter the noise of influence matrix in spatial domain.

2.2. Generating an influence matrix

In order to obtain an influence matrix for simulation, we follow the direct computation method [7], and then we will summarize the formula briefly as follows. Let a matrix $\mathbf{D}$ of dimensions $2N \times M$ denotes the influence matrix, where N and M correspond to the valid subaperture number and the actuator number, respectively. Then, the i-th column of influence matrix $\mathbf{D}$, $\mathbf{d}_i$, which can be seen as an influence vector of i-th actuator, can be calculated as follows,

$$d_{i,2k-1} = -\frac{\lambda K \iint_{S_k} \frac{\partial V_i(x,y)}{\partial x} \mathrm{d}x\mathrm{d}y}{\pi A_k} \tag{1}$$

$$d_{i,2k} = -\frac{\lambda K \iint_{S_k} \frac{\partial V_i(x,y)}{\partial y} \mathrm{d}x\mathrm{d}y}{\pi A_k} \tag{2}$$

where $d_{i,2k}$ and $d_{i,2k+1}$ refers to the $2k$-th and $(2k+1)$-th elements of $\mathbf{d}_i$, respectively, and $k = 1,2,\ldots,M$. And λ denotes the wavelength, S_k denotes the corresponding area on the DM of the k-th subaperture, A_k denotes the size of this area, and K is a constant depends on DM which denotes the variation in the central position when the actuator is actuated in a unit voltage. $V_i(x, y)$ denotes the influence function of the i-th actuator, which is defined as follows,

$$V_i(x, y) = \exp\left\{\left[\frac{1}{d}\sqrt{(x - x_i)^2 + (y - y_i)^2}\right]^{\alpha} \ln\omega\right\} \tag{3}$$

where (x_i, y_i) denotes the coordinates of the i-th actuator, d denotes the distance between neighboring actuators, α denotes the Gaussian exponent, and ω denotes the coupling coefficient.

According to this method, an influence matrix can be obtained as is shown in Fig. 1. It is worth noting that the absolute values of influence matrix are shown for the convenience of display. The axis x and axis y correspond to the M column and N row, here, we take $M = 961$ and $N = 965$ so that the configuration of this simulation and that of the experiment in Section 3 accord.

2.3. Generate influence matrices with noise

The IM generated in Section 2B can be considered to be free of noise. Subsequently, we will add noises with different variations to the influence matrix. First, we generate different pseudorandom matrices with values following standard normal distribution. As is

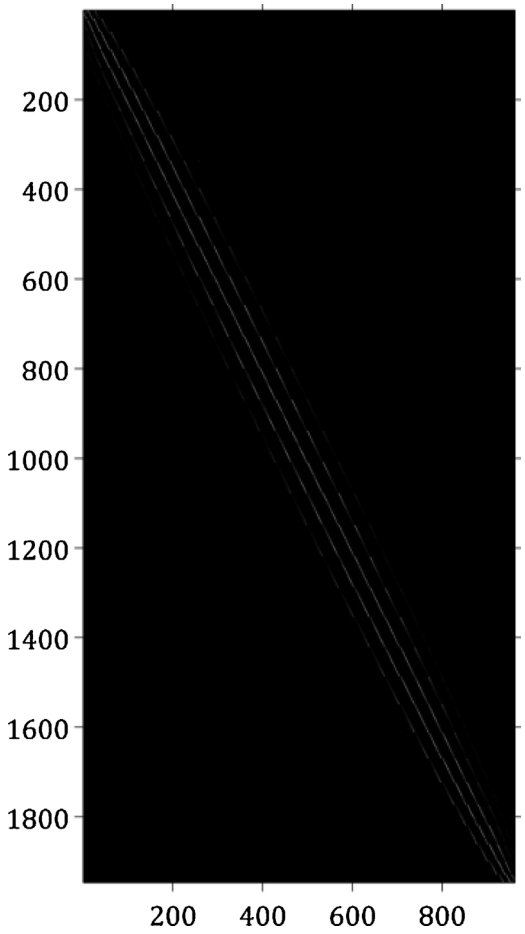

Fig. 1. Simulation results of influence matrix.

clarified by J. Kolb, the signal-to-noise (SNR) of IM can be defined as a ratio of the largest value of IM to the noise level, i.e. the standard deviation of the noise [4]. Therefore, we can obtain IMs with different SNR by adding Gaussian noise matrices with corresponding standard deviation to the original IM. Finally, 8 series of IMs are generated with different SNR ranging from 5.26 dB to 20 dB. Fig. 2 shows two typical IMs, and the SNR of them are 7.37 dB and 11.58 dB, respectively.

2.4. Filter the influence matrix in spatial domain

In this research, we adopt a filtering method in spatial domain to suppress the calibration noise in influence matrices. The core of this method is to determine the influence area on the SHWFS of each actuator. Fig. 3 shows the coupling between neighboring actuator of the 961-element DM [11], which is measured by a Zygo® interferometer. In Fig. 3, the orange dashed line indicates the position of the actuated actuator, while the blue dashed line marks the position of the neighboring un-actuated actuator. It is worth noting that one actuator is only coupled with neighboring actuators. For convenience of understanding, Fig. 4 explains the influence area of a central actuator which is seen by SHWFS. In Fig. 4, the big dashed circles correspond to the subapertures of SHWFS, the small circles mark the positions of the spots of SHWFS, and the small squares indicate the corresponding positions on the SHWFS of the actuators. Easy to find that an actuator mainly influence the corresponding subaperture and the eight-neighboring subaperture of that. Therefore, we consider the 3-by-3 subapertures, which is indicated by a red dashed square, as the influence square of an actuator.

Thus, we can define a filter matrix $\mathbf{\Delta}$ of dimension $2N \times M$, and the element of $\mathbf{\Delta}$ can be determined as follows,

$$\delta_{i,2k} = \begin{cases} 1 & \text{if the } k\text{-th subaperture belongs to} \\ & \text{the influence area of the } i\text{-th actuator} \\ 0 & \text{else} \end{cases} \tag{4}$$

$$\delta_{i,2k} = \delta_{i,2k-1} \tag{5}$$

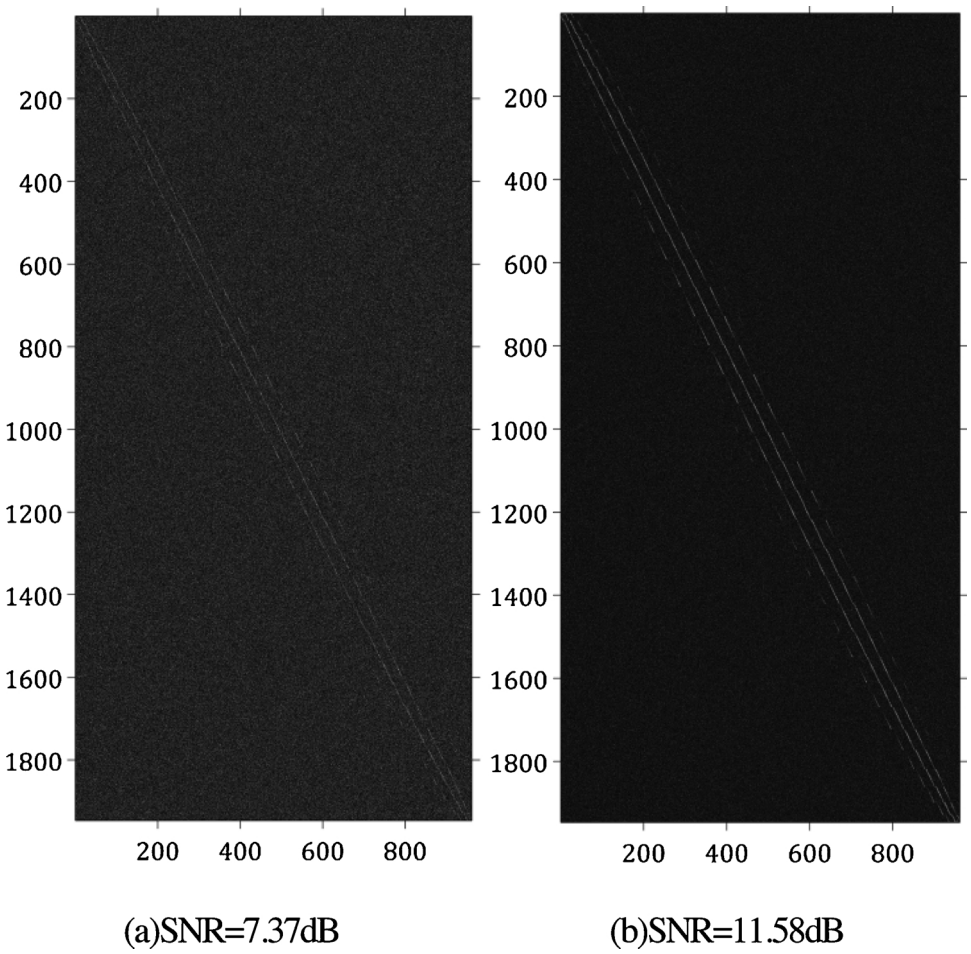

Fig. 2. Influence matrix with Gaussian noise.

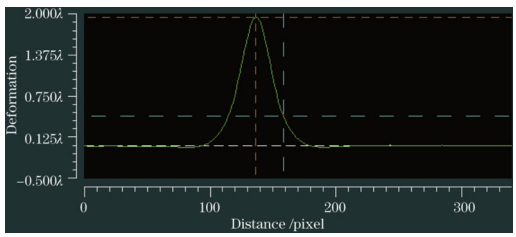

Fig. 3. The coupling between neighboring actuator of 961-element DM.

where $i = 1, 2, \ldots, M$, and $k = 1, 2, \ldots, N$. Then, the filtering process is,

$$\hat{\mathbf{D}} = \mathbf{D} \bullet \boldsymbol{\Delta} \tag{6}$$

where $\hat{\mathbf{D}}$ refers to a filtered influence matrix.

There are other style of filtering methods, such as the one adopted by S. Cheng, and the strategy of that is ignoring all the elements of IM which is less than one percent of the maximum element [15]. In this article, we just focus on the spatial-domain filtering.

2.5. Conducting a closed-loop wavefront correction

In order to test the effects of filtering, we conduct a simulation of a closed-loop wavefront correction using both the filtered matrices and the unfiltered matrices of the IMs which are generated with noise in Section 2C. Here, an integrator control strategy is adopted, and the integrator gain is set to 0.3 for all the simulations. The initial aberrations are shown in Fig. 5, which is similar to those in the practical HOAO experimental system in Section 3. The RMS of the aberration is about 3.03λ.

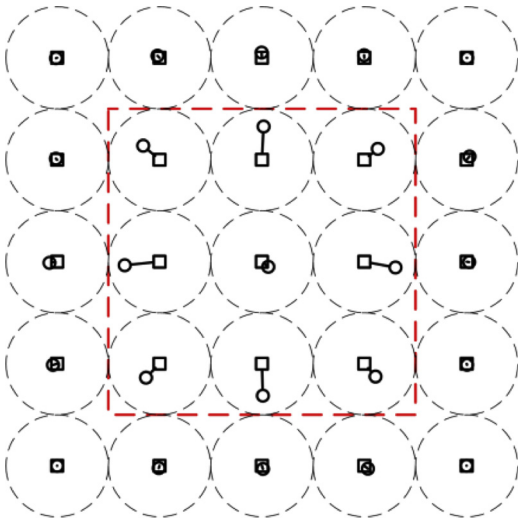

Fig. 4. The influence of the central actuator on the SHWFS.

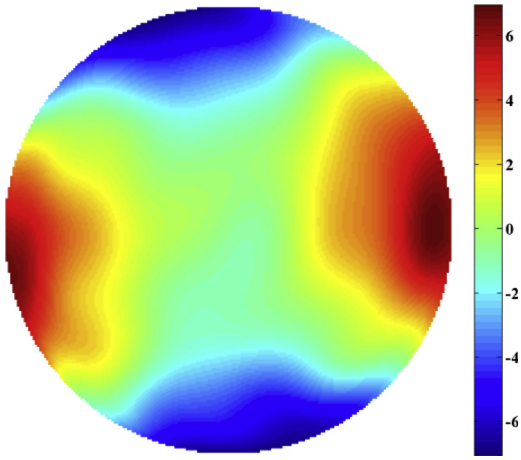

Fig. 5. Initial aberrations for closed-loop correction (in λ).

Then, Fig. 6 shows the residual aberration curves of wavefront correction process under eight different SNRs, ranging from 5.26 dB to 20.00 dB. From the curves, it can be found that the calibration noise in IMs deteriorate the HOAO system performance considerably. With respect to the filtering method, generally speaking, the filtered matrices work much better than the unfiltered matrices. For the filtered matrices, the residual aberration curves begin to converge when the SNR reaches 11.58 dB, while for the unfiltered matrices, the curves start to converge until the SNR reaches 16.79 dB. It is worth noting that the convergence rates are much more rapid and the wavefront correction processes are more stable with the filterer matrices than with the unfiltered matrices, for higher SNRs. Also, the curves with unfiltered matrices absolutely diverge for lower SNR, such as 9.47 dB, while those with filtered matrices not. The simulation of the closed-loop wavefront correction validates the effectiveness of the filtered method.

3. Experiments

3.1. Experiment setup

In order to test the filtering method in practical adaptive optics systems, we construct a experimental HOAO system by using the 961-element DM, the SHWFS based on a Basler® camera, and a collimation optics system. The parameters of SHWFS and DM have been discussed in Section 2A. The schematic of the system is shown as Fig. 7. As is similar to the simulations above, the integrator gain as set to 0.3 as well in the experiments.

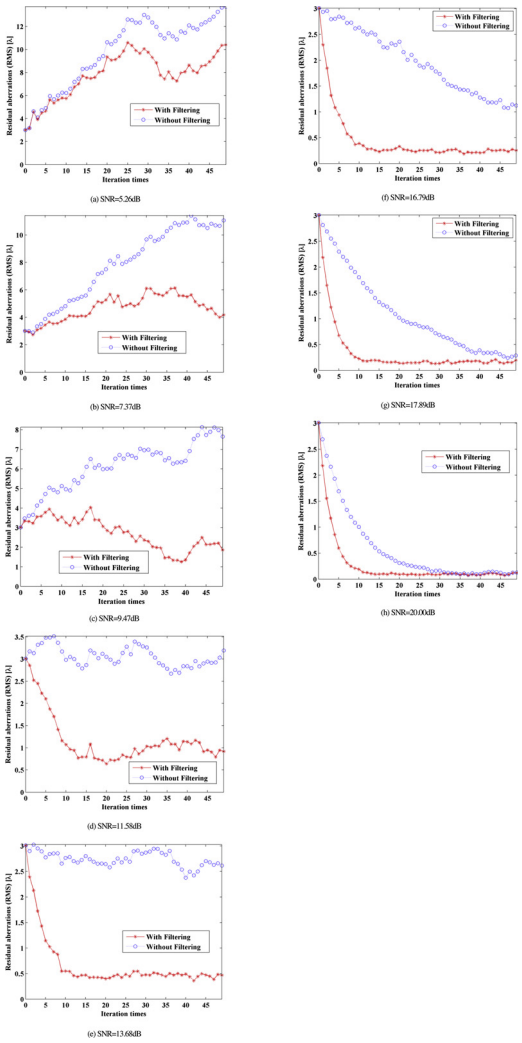

Fig. 6. Curves of residual aberrations in closed-loop wavefront correction simulations.

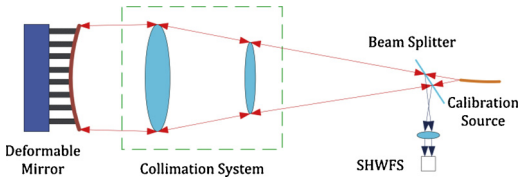

Fig. 7. Schematic of adaptive optics experimental system.

3.2. Experiment results

We conduct two closed-loop wavefront correction experiments by using an IM which is measured practically in this HOAO experimental system. In the first experiment, the spatial-domain filtering method is adopted to process the measured IM, and then, the filtered IM is used in the closed-loop experiment. In the second experiment, the measured IM is used in the closed-loop experiment directly.

Fig. 8 shows the residual aberration curves in two closed-loop experiments in which the static aberrations are corrected. The initial aberrations are shown in Fig. 9(a), and the RMS of the aberrations is about 2.307λ. Similar to the simulation results in Fig. 6, for the filtered IM, the convergence rate is much more rapid than that for the Unfiltered one. Fig. 9(b) shows the results after wavefront correcting by using the filtered IM. Therefore, the experiments have prove the effectiveness of the filtering method.

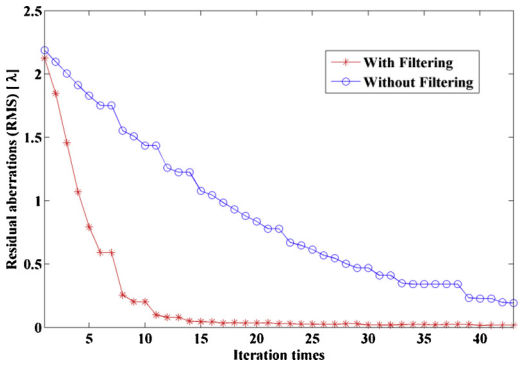

Fig. 8. Curves of residual aberrations in closed-loop wavefront correction experiments.

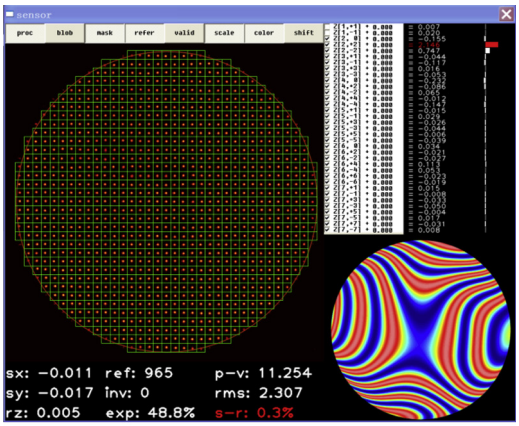

(a) SHWFS results before wavefront correcting

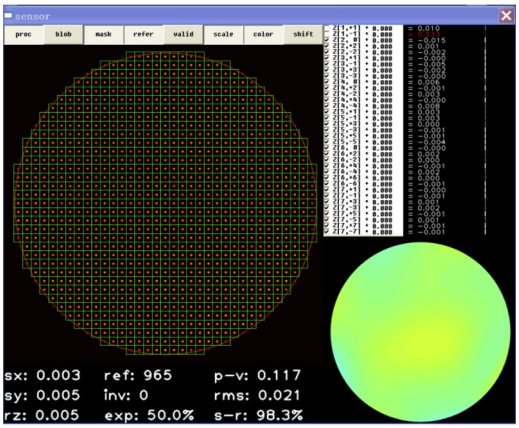

(b) SHWFS results after wavefront correcting

Fig. 9. SHWFS results in a closed-loop wavefront correcting with the filtered influence matrix.

4. Conclusions

The calibration noise exists in influence matrices of high-order adaptive optics system. In this article, taking an adaptive optics system which contains a 961-element deformable mirror as a example, the influence of calibration noise are analyzed and a filtering strategy is researched by using numerical simulations and practical experiments, respectively. In the numerical simulation, an influence matrix is generated through the direct computation method, and Gaussian noises of different standard variations are added to this influence matrix so that influence matrices of different SNRs can be obtained. Then, a filtering method in the spatial domain is used to process the influence matrices with noise, and closed-loop wavefront corrections are conducted. The results of the numerical

simulation show that the calibration noise in influence matrix deteriorate system performance considerably. The numerical simulation also shows that the wavefront correction converge when the SNR is above 11.58 dB, for the filtered matrix; however, for the unfiltered matrix, the wavefront correction does not converge until the SNR reaches 16.79 dB. Finally, a practical experiment is carried out and the results show that the convergence rate is much more rapid for the filtered matrix, which are in accord with the simulation results. Both the simulations and the experiments have validate the effectiveness of the spatial-domain filtering method.

In the future research, we can try to apply the methods to analyze the influence matrix of other types of adaptive optics system [16,17].

Acknowledgments

This work was supported by the Excellent Young Scientists Fund of the Science and Technology Development Foundation of Jilin Province, China (No. 20180520076JH) and the National Natural Science Foundation of China (No.11703024).

We are also very grateful to prof. Hongzhuang Li and prof. Xudong Lin for their work in developing the SHWFS and the deformable mirror, respectively, in this research.

References

[1] J.-F. Sauvage, T. Fusco, C. Petit, A. Costille, D. Mouillet, J.-L. Beuzit, K. Dohlen, M. Kasper, M. Suarez, C. Soenke, A. Baruffolo, B. Salasnich, S. Rochat, E. Fedrigo, P. Baudoz, E. Hugot, A. Sevin, D. Perret, F. Wildi, M. Downing, P. Feautrier, P. Puget, A. Vigan, J. O'Neal, J. Girard, D. Mawet, H.M. Schmid, R. Roelfsema, SAXO: the extreme adaptive optics system of SPHERE (I) system overview and global laboratory performance, J. Astron. Telesc. Instrum. Syst. 2 (2016) 025003.
[2] K. Wagner, D. Apai, M. Kasper, K. Kratter, M. McClure, M. Robberto, J.-L. Beuzit, Direct imaging discovery of a Jovian exoplanet within a triple-star system, Science 353 (2016) 673.
[3] C. Boyer, V. Michon, G. Rousset, Adaptive optics: interaction matrix measurements and real time control algorithms for the COME-ON project, Proc. SPIE 1237 (1990) 406.
[4] J. Kolb, Review of AO calibrations, or how to best educate your AO system, Proc. SPIE 9909 (2016) 99090K.
[5] M. Kasper, E. Fedrigo, D.P. Looze, H. Bonnet, L. Ivanescu, S. Oberti, Fast calibration of high-order adaptive optics systems, J. Opt. Soc. Am. A 21 (2004) 1004.
[6] Y. Guo, C. Rao, H. Bao, A. Zhang, X. Zhang, K. Wei, Multichannel-Hadamard calibration of high-order adaptive optics systems, Opt. Express 22 (2014) 13792.
[7] Y. Guo, C. Rao, H. Bao, A. Zhang, K. Wei, Direct computation of the interaction matrix of adaptive optical system, Acta Opt. Sin. 63 (2014) 149501(in Chinese).
[8] S. Meimon, C. Petit, T. Fusco, Optimized calibration strategy for high order adaptive optics systems in closed-loop: the slope-oriented Hadamard actuation, Opt. Express 23 (2015) 27134.
[9] A. Chiuso, R. Muradore, E. Marchetti, Dynamic calibration of adaptive optics systems: a system identification approach, IEEE Trans. Control. Syst. Technol. 18 (2010) 705.
[10] C.T. Heritier, S. Esposito, T. Fusco, B. Neichel, S. Oberti, R. Briguglio, G. Agapito, A. Puglisi, E. Pinna, P.-Y. Madec, A new calibration strategy for adaptive telescopes with pyramid WFS, Mon. Not. R. Astron. Soc. 481 (2018) 2829.
[11] X. Lin, X. Liu, J. Wang, H. Li, F. Wang, P. Wei, L. Wang, K. Yao, J. Jia, Development and performance test of the 961-Element deformable mirror, Acta Opt. Sin. 33 (2013) 0601001(in Chinese).
[12] L. Wang, T. Chen, X. Liu, X. Lin, X. Yang, H. Li, Stability evaluation and improvement of adaptive optics systems using lyapunov stability approach, J. Kor. Phys. Soc. 68 (2016) 486.
[13] L. Wang, T. Chen, X. Lin, P. Wei, X. Liu, J. Jia, Performance measurement of adaptive optics system based on Strehl ratio, J. China Univ. Posts Telecommun. 23 (2016) 94.
[14] L. Wang, X. Lin, X. Liu, P. Wei, Adaptive optics system based on the Southwell geometry and Improvement on control stability, Opt. Commun. 390 (2017) 105.
[15] S. Cheng, W. Liu, S. Chen, L. Dong, P. Yang, B. Xu, Comparison between iterative wavefront control algorithm and direct gradient wavefront control algorithm for adaptive optics system, Chin. Phys. B 24 (2015) 084214.
[16] Z. Fan, J. Qiu, Z. Kang, Y. Chen, W. Ge, X. Tang, High beam quality 5 J, 200 Hz Nd:YAG laser system, Light Sci. Appl. 6 (2017) e17004.
[17] R. Florentin, V. Kermene, J. Benoist, A. Desfarges-Berthelemot, D. Pagnoux, A. Barthélémy, J.-P. Huignard, Shaping the light amplified in a multimode fiber, Light Sci. Appl. 6 (2017) e16208.